Available online at www.dergipark.gov.tr

INTERNATIONAL ADVANCED RESEARCHES and ENGINEERING JOURNAL

Journal homepage: www.dergipark.gov.tr/iarej

e-ISSN: 2618-575X

International Open Access

Volume 03
Issue 01

April, 2019

Research Article

Biosynthesis and characterization of iron oxide nanoparticles from *Enteromorpha spp.* extract: determination of adsorbent properties for copper (II) ions

Gizem Ercan [a], ***Deniz Uzunoğlu*** [a], ***Memduha Ergüt*** [a,*] ***and Ayla Özer*** [a]

[a] *Mersin University, Department of Chemical Engineering, Mersin 33343, Turkey*

ARTICLE INFO

Article history:
Received 13 March 2018
Accepted 12 October 2018

Keywords:
Biosynthesis
Cu^{2+} adsorption
Enteromorpha spp.
Iron oxide nanoparticles
Marine algae

ABSTRACT

Iron oxide nanoparticles (IO-NPs) were synthesized via a biosynthesis method using marine algae *Enteromorpha spp.* extract as a biological reductant agent in this study. Moreover, the total phenolic content of *Enteromorpha spp.* was found as 9.81± 4.8 mg gallic acid equivalents/g dry algae. The biosynthesized IO-NPs were characterized by zeta potential, DLS, SEM/EDX, and FTIR analysis methods and also the formation of IO-NPs was approved with the UV-vis spectrum. The characteristic surface plasmon resonance (λ_{SPR}, nm) value showing the formation of IO-NPs was observed at nearly 410 nm in terms of UV–vis analysis. According to DLS analysis results, the mean hydrodynamic diameter of IO-NPs was determined as 78.83 nm. According to SEM results, spherical nanoparticles are formed, and EDX analysis showed that the signals in the Fe and O elements confirmed the formation IO-NPs. According to FT-IR analysis results, the formation of IO-NPs was approved by the absorption bands at 599.83, and 475 cm^{-1}, which corresponded to the Fe-O stretches of Fe_3O_4 and Fe_2O_3. Subsequently, the synthesized IO-NPs were utilized as an adsorbent for the removal of Cu^{2+} from aqueous solutions. Batch adsorption experiments were conducted to examine the optimum adsorption environmental conditions and the equilibrium, kinetics, and mass transfer modeling was also evaluated. The optimum adsorption conditions were found as initial pH 5.0; temperature 35°C, initial Cu^{2+} concentration 275 mg/L, and adsorbent concentration 0.5 g/L. The experimental equilibrium data were in the best agreement with Langmuir isotherm model, and the maximum monolayer coverage capacity of IO-NPs for Cu^{2+} adsorption found to be 188.68 mg/g at optimum temperature value of 35°C. The adsorption kinetic data were consistent with the pseudo second order kinetic model, and Weber Morris model showed that both the film (boundary layer) and intraparticle diffusion affected the adsorption process.

1. Introduction

Copper (II) have been frequently used in several industries like metal cleaning, paints and pigments, paper board, fertilizer, plating baths, and wood pulp. So, it is one of the best known non-biodegradable water pollutants which are causing serious soil and water pollution. Moreover, Copper (II) is extremely toxic and dangerous for ecosystem, agriculture and human health.

The acceptable discharge limit of copper in industrial wastewaters is reported as 1.0 mg/L by the US Environmental Protection Agency [1]. Therefore, to reduce Cu^{2+} to the standard level, effective, eco-friendly and economic treatment methods are being developed by researchers. There are commonly used treatment methods for discharging copper ions from wastewaters such as ion exchange, adsorption, extraction, reverse osmosis, coagulation, chemical precipitation, and membrane filtration techniques. Among them, adsorption is a frequently-preferred method for heavy metals removal from the wastewaters due to its simple operation, low cost, the capability of trace level pollutant removal and high efficiency [2].

Recently, the usage of metal/metal oxide nanoparticles as an adsorbent has attracted great attention for treatment

* Corresponding author. Tel.: +90-324-361-0001/17371; Fax: +90-324-361-0032
E-mail address: gizemercan16@gmail.com *(G. Ercan)*, denizuzunoglu4@gmail.com *(D. Uzunoğlu)*, memduha.ergut@mersin.edu.tr *(M. Ergüt)*, ayozer4@gmail.com *(A. Özer)*
ORCID: *0000-0002-2496-7887 (G. Ercan), 0000-0001-9706-303X (D. Uzunoğlu), 0000-0001-7297-1533 (M. Ergüt), 0000-0002-7824-238X (A. Özer)*

of various heavy metals. The advantage of these nanomaterials is high adsorption capacity that is associated with their large specific surface area and high reactivity in the adsorption processes [3]. In this respect, the biosynthesis methods which is environmentally friendly and do not include dangerous substances in the synthesis step have begun to gain importance for the synthesis of metal nanoparticles. Biological methods that are using enzymes, microorganisms, alga, and plants, have been used as practicable environmentally-friendly and safer than other chemical and physical methods which are risky and expensive [4].

Marine algae are divided into macroalgae and microalgae. Marine macroalgae, in other word seaweed, are planted like organisms. They are categorized into three groups considering their pigmentation as brown (phaeophytes), red (rhodophytes), and green (chlorophytes) which are located in the marine or saltwater environment. The latest studies indicated that marine algae could be used for the synthesis of metal nanoparticles owing to their phytochemicals. These phytochemicals include various functional groups such as; amino, hydroxyl, and carboxyl which could act as effective metal-reducing agents [4, 5].

The present study aimed to synthesize iron oxide nanoparticles (IO-NPs) using seaweed *Enteromorpha spp*. algal extract as a reducing/capping agent and to investigate the adsorption of copper (II) ions to IO-NPs.

2. Materials and Methods

2.1 Preparation of Algal Extract from Enteromorpha spp.

The green algal genus *Enteromorpha spp.* was picked up from Mediterranean coastline in Mersin, Turkey. Specimens of green seaweed were firstly rinsed with tap water and then washed with pure water. After that, they were dried in an oven at 60°C for 2 h. For the preparation of extract, 5 g of the washed and dried algae samples were boiled in 600 mL of pure water in a beaker under continuously stirring for 180 min. The prepared extract was cooled to room temperature, and then the insoluble fractions and macromolecules were removed by centrifuging the extract. Finally, the obtained green colored extract was kept in the refrigerator at +4°C for the nanoparticle synthesis and the analysis studies.

2.2 Determination of Total Phenolic Content of Enteromorpha spp. extract

In order to determine the total phenolic content (TFC) of *Enteromorpha spp*. extract, the Folin-Ciocalteu colorimetric method adapted from Slinkard and Singleton (1977) was applied [6]. According to the method, 100 µL Folin-Ciocalteu reagent and 1.4 mL of distilled water were put into 200 µL of the extrac, and the formed solution was agitated well. After 2 min, 300 µL of 20% (w/v) Na_2CO_3 solution was added to the present solution. Tube content was vortexed again and then left to wait for 2 h at room temperature in the dark. TFC of the extract was stated as gallic acid equivalent (µg of gallic acid/g dry leaf). To determine TFC value, the absorbance of the blue colored solution was recorded at 765 nm with UV–Vis spectrophotometer. For this purpose, a calibration curve (R^2 = 0.996) was formed firstly at different concentrations (100 – 700 mg/L) of gallic acid, and then, TFC value of the extract was observed using the absorbance values. The results were reported as the average of three absorbance measurements.

2.3 Synthesis of Iron Oxide Nanoparticles

Iron oxide nanoparticles (IO-NPs) were synthesized via biosynthesis method by using *Enteromorpha spp.* algal extract as a natural reductant/capping agent. The green colored extract was added drop by drop manually into 0.1 M $FeCl_3$ solution in a 1:2 volume ratio at room temperature and then the color of the yellow solution turned to brown with the creation of nanoparticles in a short time. After that, the resulting nanoparticles were filtered with Whatman # 1 filter paper and dried in an oven at 80°C for 4 h. IO-NPs were crumbled homogeneously by handle-mortar and were kept in closed vessels in a refrigerator at +4°C for further experiments [7]. Biosynthesized IO-NPs were characterized by zetasizer (Malvern, UK) using Dynamic Light Scattering (DLS) technique, zeta potential analyzer (Malvern, UK), UV-vis spectrophotometer (Specord 210 Plus-Analytic Jena, Germany), and Fourier Transform Infrared Spectrometer (FTIR- Perkin Elmer, Shelton).

2.4 Preparation of Cu^{2+} solutions

In order to prepare the stock solution of Cu^{2+} (1.0 g/L), 3.9292 g of $CuSO_4.5H_2O$ was dissolved in 1 L of distilled water. The solutions at different concentrations of Cu^{2+} (50–500 mg/L) were prepared with required dilutions from the stock solution. The initial pHs of the solutions were fixed up to the desired value with 0.1 M solutions of NaOH and HCl.

2.5 Batch adsorption studies

The experiments of Cu^{2+} ions adsorption onto IO-NPs were done in a batch system with artificial wastewater. Two parallel experiments were performed for each adsorption study. The adsorption experiments were conducted in 250 mL Erlenmeyer flasks containing 100 mL of adsorbate solution involving Cu^{2+} ions. 0.1 g of IO-NPs was added to 100 mL of Cu^{2+} solution at the desired initial pH and Cu^{2+} ion concentration. The flasks were shaken in an agitation vessel at the constant

temperature for 210 min to achieve adsorption equilibrium. At foregone time intervals (0.0, 0.5, 2.0, 5.0, 10, 20, 30, 60, 90, 120, 150, 180, and 210 min), the samples from the adsorption solution were taken and centrifuged at 4000 rev/min for 3.0 min. For different environmental conditions such as initial pH, initial Cu^{2+} ion concentration, adsorbent concentration, and temperature, the adsorption experiments were repeated and the experimental data were observed.

2.6 Cu^{2+} analysis

The unadsorbed Cu^{2+} ion concentration in the supernatant was analyzed spectrophotometrically [1]. 1.5 N of 20 mL NH_3 solution and 1% (w/v) of 0.2 mL sodium diethyl di-thio-carbamate solution were put into 1 mL of the supernatant, and it was diluted to 25 mL with pure water. After the yellow-brown solution formed, it was analyzed in terms of UV-vis spectrophotometer at 460 nm. The adsorbed Cu^{2+} ion amounts at equilibrium (q_e (mg/g)) and the adsorption percentages (adsorption, %) were calculated as follows:

$$q_e = (C_o - C_e)/X_o \quad (1)$$

$$\text{Adsorption percentage (\%)} = ((C_o - C_e) / C_o) \times 100 \quad (2)$$

where C_o is the initial concentration (mg/L), and C_e is the equilibrium concentration and X_o is the adsorbent concentration (g/L).

3. Results and Discussions

3.1 Characterization of IO-NPs

The effective hydrodynamic diameter distribution of IO-NPs was analyzed by DLS technique, and the results were represented in Figure 1. According to Figure 1, the smallest IO-NPs (58.77 nm) had the distribution of 10.4 % while the single IO-NPs with the effective hydrodynamic diameter of 78.82 nm were the most frequent ones (32.7 %). Consequently, the mean diameter of IO-NPs was determined as 78.83 nm.

The formation of IO-NPs was firstly noted by visual observation of the color of [IO-NPs-algae extract] solution, and then the UV-vis spectra of the solution were recorded against pure water with 1 mm optical path length quartz cuvette. Accordingly, the color of the solution altered from yellow to brown with the creation of nanoparticles due to the surface plasmon resonance (λ_{SPR}, nm) phenomenon. According to Figure 2, a characteristic and distinct λ_{SPR} value of IO-NPs was obtained at nearly 410 nm.

The SEM images of the synthesized IO-NPs were presented in Figure 3(a) and (b) before and after adsorption, respectively. As seen from Figure 3(a), the nanoparticles have spherical and porous morphology and agglomerated. Moreover, the mean hydrodynamic particle size of IONPs was calculated to be 62 nm by using the Image J program using randomly selected 50 particles from SEM images. The mean hydrodynamic diameters of nanoparticles were found a bit higher than DLS analysis results may be due to the absorption effects and particle scattering because of agglomeration. After Cu^{2+} adsorption, as shown in Figure 3(b), a smooth surface was obtained. The nanoparticles were more agglomerated, and the pores were closed because of the adsorption of Cu^{2+} ions onto the surface of the adsorbent.

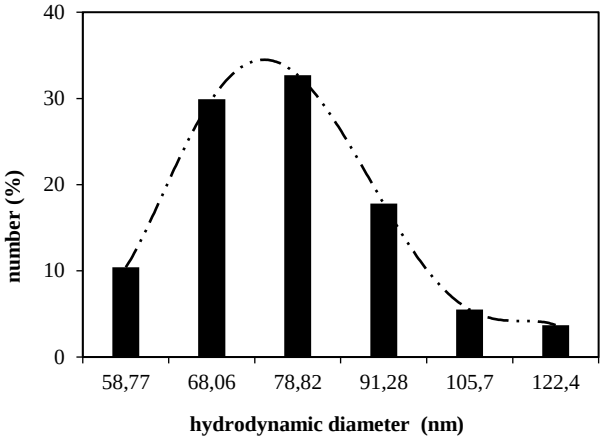

Figure 1. The effective hydrodynamic diameter distribution of IO-NPs

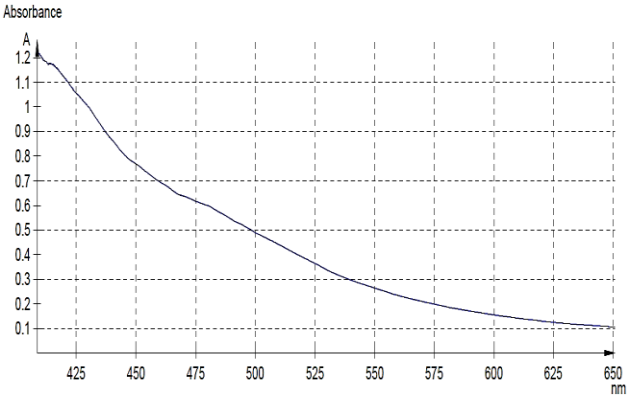

Figure 2. UV-vis spectra of [IO-NPs-algae extract] solution

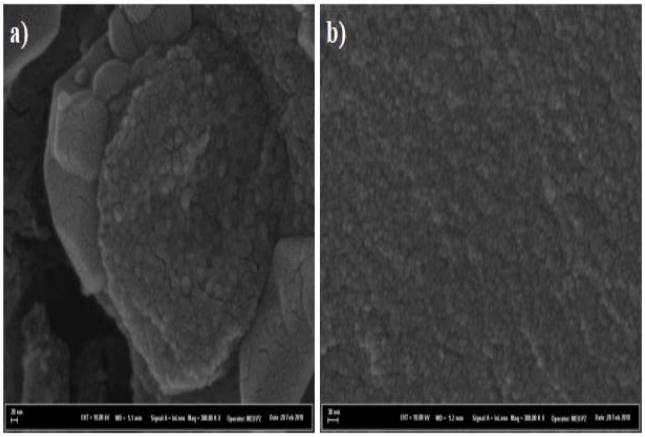

Figure 3. SEM images of IO-NPs (a) before and (b) after adsorption

According to EDX analysis results, the elemental and quantitative weight composition (wt.%) of synthesized IO-NPs was composed of 33.05 % Fe, 32.96 % O, 15.53 % C, 7.02 % Na, 3.68 % S, 3.12 % Cl, 2.59 % N, 1.24% Mg and 0.84% Ca elements. Elemental analysis (EDX) spectrums of IO-NPs before and after adsorption were given in Figure 4(a) and (b) respectively. According to Figure 4(a), the prepared IO-NPs involve the elements of Fe, O, C, Na, S, Cl, N, Ca, and Mg (the peaks of the elements of Pt and Pd stem from the coating of the sample), before adsorption. EDX analysis results revealed that the signals in the Fe and O elements confirmed the formation IO-NPs, whereas the elements of C, a part of O, Na, S, Ca and Mg derived from the aqueous algal extract. The presences of these elements ascribed to the polyphenol groups and other C-containing molecules [8]. Also, Cl element must be arisen from $FeCl_3$ precursor used in IO-NPs synthesis. After adsorption, in addition to Fe, O, C, N, S, Na, Ca and Mg elements also, Cu element was detected in EDX analysis results after adsorption. The presence of Cu element in the elemental composition confirmed the binding of the Cu^{2+} ions onto IO-NPs surface.

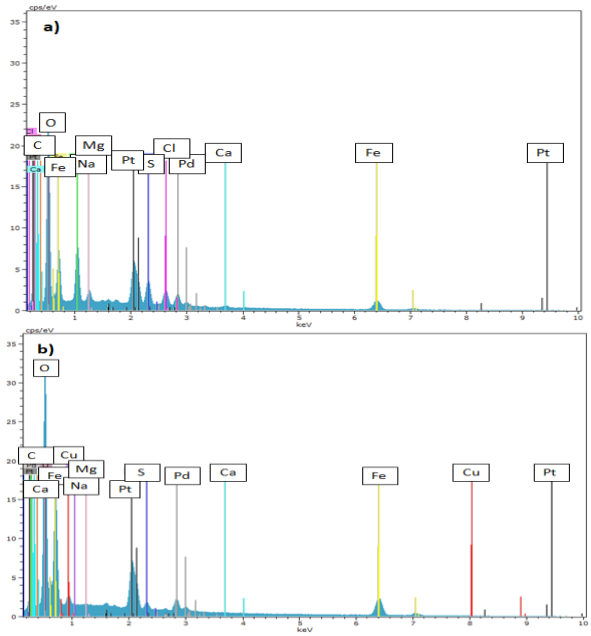

Figure 4. EDX spectrum of IO-NPs a) before and b) after adsorption

The FT-IR spectrum of the synthesized IO-NPs before and after Cu^{2+} adsorption was exhibited in Figure 5. As shown in Figure 5, no important changes in the structures were observed between pre- and post-adsorption. According to the FT-IR spectrum of biosynthesized IO-NPs (Figure 5.a), the broad band at between 3200–3300 cm^{-1} is attributed to O-H stretching vibration. The slight bands at 2030 and 2187 cm^{-1} related to C-H stretching vibration of $-CH_2$ and $-CH_3$ functional groups. The stretching vibration band at 1216 cm^{-1} is due to the characteristic asymmetric stretching vibration of the sulfate group. Sulfate, carboxyl, hydroxyl, and amino groups are bioactive compounds that exist in a marine alga. These functional groups can be responsible for the formation of nanoparticles. For instance, it was indicated that the sulfated polysaccharides isolated from the marine alga had a powerful capability to synthesize nanoparticles. Therefore, the sulfate group may be responsible for the reduction of iron ions by oxidation of aldehyde groups to carboxylic acids [4]. The band at 1039.55 cm^{-1} is identified as the symmetric C–O vibration related to a $C–O–SO_3$ group. These peaks demonstrate the presence of sulfated polysaccharides in the *Enteromorpha spp.* algal extract. Therefore, *Enteromorpha spp.* algal extract containing hydroxyl, sulfate, and aldehyde groups may result in the reduction of Fe^{3+} and synthesis of IO-NPs. Moreover, the peak at 1617.53 cm^{-1} corresponds to the conjugated carbonyl (NH) (–C=O) group stretching vibration that is characteristic of proteins. This peak became slight broader and slightly shifted from 1622.05 cm^{-1}. The result showed a member of (NH) (–C=O) group within the cage of cyclic peptides acting a role in stabilizing the nanoparticles [5]. Another peak at 1400 cm^{-1} represents the C-C groups result from aromatic rings that are involved in the algal extract. The formation of IO-NPs was characterized by the absorption bands at 599.83 and 475 cm^{-1} which related to the Fe-O stretches of Fe_3O_4 and Fe_2O_3 [9], confirming the formation of IO-NPs.

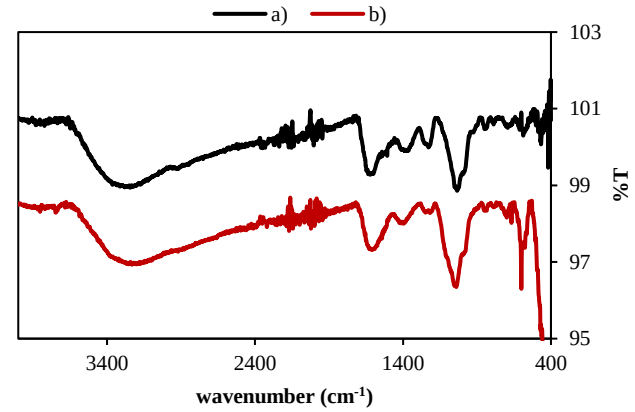

Figure 5. The FT-IR spectrum of the biosynthesized IO-NPs a) before adsorption b) after adsorption

3.2. Total phenolic content of Enteromorpha spp. extract

The polyphenols in many plants and alga contain mainly flavonoids (flavonols, flavones, flavanones, isoflavones, flavanols, and anthocyanins) and phenolic acids (hydroxycinnamic and hydroxybenzoic acids). They are synthesized as a defense mechanism against microorganisms, and they have shown hydrogen-donor potentials and metal chelation abilities [10]. Many studies

which are based on the green synthesis of metal/metal oxide nanoparticles, fundamentally cited that plants and alga with high polyphenolic content had a capping/stabilizing ability to reduce metal precursors to their nanoforms [11]. Therefore, TFC of *Enteromorpha spp.* extract was determined to show the potential of reducing capability for IO-NPs synthesis. TFC of *Enteromorpha spp.* extract was determined as 9.81± 4.8 mg gallic acid equivalents/g dry algae. Some studies about the phenolic content of *Enteromorpha* species reported in the literature. Ganesan et al., [12], investigated TFC of three species of green seaweed *Enteromorpha (E. compressa, E. linza, and E. tubulosa).* They found the total phenol content (%), calculated with a phloroglucinol standard, in the extract of water as (2.98 ± 0.39), (1.33 ± 0.08) and (1.33 ± 0.08) for *E. compressa, E. linza* and *E. tubulosa* respectively. In another study, the phenolic content of *Enteromorpha intestinalis (L.) Kütz.* seaweed, collected from Acıgöl Lake in Turkey, was investigated by Akköz et al., [13]. The researchers found TFC of it was 0.025± 0.004 mg gallic acid equivalent/g dry algae. Our study showed that TFC of *Enteromorpha spp.* grown in Mediterranean Sea of Turkey seems significantly high, therefore owing to its high phenolic content, *Enteromorpha spp.* extracts can be used as a bioreductant for preparing metal nanoparticles owing to their reducing capability of metal salts. Consequently, the IO-NPs were synthesized successfully by using *Enteromorpha spp.* extract as a non-toxic, cost-effective, and an environmentally friendly reductive agent.

3.3 Effect of environmental conditions to adsorption

3.3.1 Initial pH

The initial pH value of aqueous solution containing heavy metal ions is a significant factor affecting the adsorption processes. Because, the dissolution of metal, as well as the activity of such as amino, carboxyl, sulfate, and phosphate functional groups that present on adsorbent, are affected from pH [14]. The effect of initial pH on the adsorption of Cu^{2+} ions onto IO-NPs was presented in Figure 6. As shown in Figure 6, the maximum equilibrium uptake value was observed at pH 5.0. The maximum adsorption capacity at the initial pH 5.0 could be defined by the interaction of Cu^{2+} ions and surface charge of adsorbent. The net surface charges of synthesized IO-NPs were determined by measuring ζ (zeta) potential in the pH range of 2.0–6.0 and the change of ζ potential with pH were presented in Figure 7. As shown in Figure 7, it was determined that the IO-NPs surface was negatively charged for all pH values and had a maximum negative charge at pH 5.01 (-33.7 mV). So, the adsorbed Cu^{2+} amount was maximum due to strong electrostatic attractions between Cu^{2+} cations and negatively charged surface at pH 5.0. The aforementioned electrostatic attraction was illustrated in Figure 8, similar to previously proposed by Brunkesh et al., [15].

3.3.2 Initial Cu^{2+} ion concentration

The effect of initial Cu^{2+} ion concentration on the adsorption was shown in Figure 9. From Figure 9, it was indicated that the uptake amounts at equilibrium increased with increase in the experimental initial Cu^{2+} ion concentration up to 275 mg/L, and then remained constant after that as a result covering of active sites of IO-NPs with the Cu^{2+} ions.

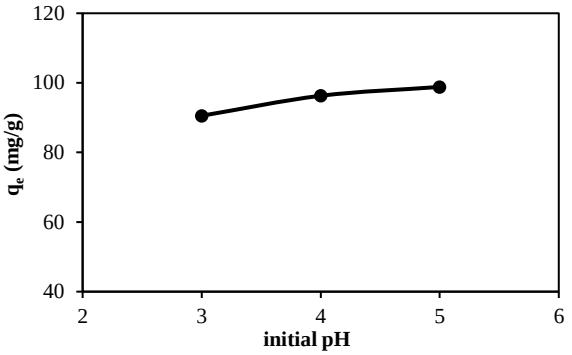

Figure 6. Effect of initial pH (T=25°C, C_o=100 mg/L, X_o=1 g/L)

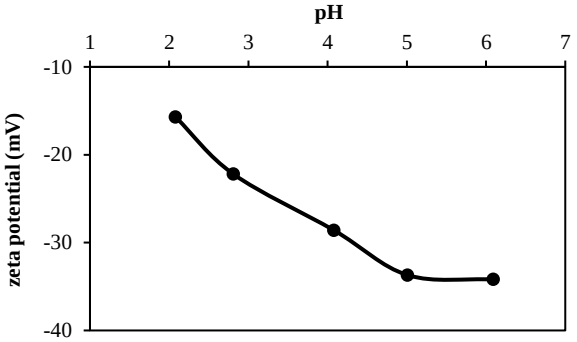

Figure 7. The plot of zeta potential value of the synthesized IO-NPs vs. pH

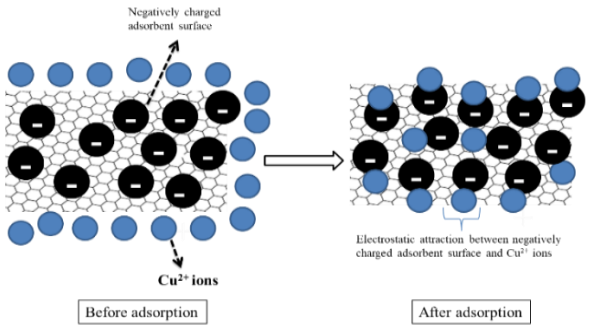

Figure 8. The proposed mechanism of Cu^{2+} adsorption onto IO-NPs

However, the adsorption percentages decreased with increase in the experimental initial Cu^{2+} ion concentration

because of the high ratio of initial Cu^{2+} ion concentration to the available adsorption surface area. Thus, the optimum Cu^{2+} ion concentration was found as 275 mg/L.

3.3.3 Adsorbent concentration

The adsorbent concentration effect on the equilibrium uptake and percentage of adsorption was presented in Figure 10. According to Figure 10, the equilibrium uptakes of Cu^{2+} ion concentrations increased with decreasing the adsorbent concentration from 3.5 g/L to 0.5 g/L. Also; the adsorption percentage slightly increased up to 2.0 g/L of adsorbent concentration, and then indistinctly remained constant with further increase in adsorbent concentration. The increase in uptake values with decreasing adsorbent concentration may arise from the interaction between adsorbent particles such as aggregation, resulting from high adsorbent concentration. The higher adsorption capacities were obtained at lower adsorbent concentrations due to the agglomeration of the adsorbent particles. The agglomeration would cause a decrease in the active surface area of the adsorbent and an increase in diffusional path length. Consequently, the optimum adsorbent concentration was selected to be 0.5 g/L for Cu^{2+} ion adsorption onto IO-NPs.

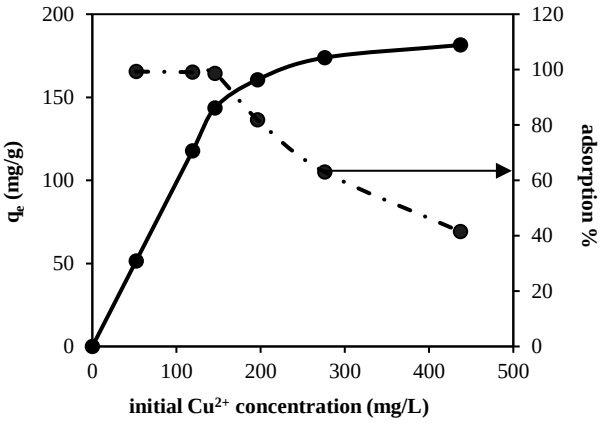

Figure 9. Effect of initial Cu^{2+} concentration (initial pH= 5, T=35°C, X_o=1 g/L)

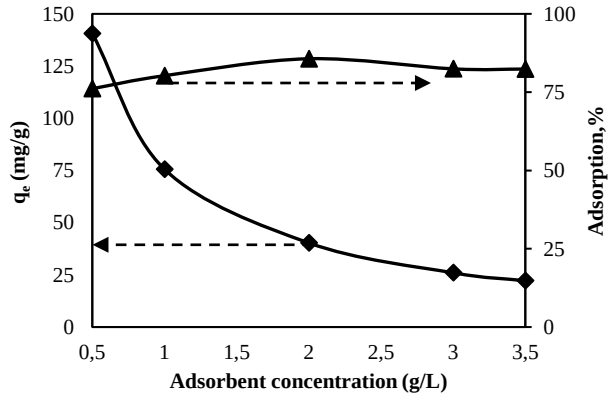

Figure 10. Effect of adsorbent concentration (initial pH= 5, T= 35°C, C_o=100 mg/L)

3.3.4 Temperature

The variation of the adsorption capacities of IO-NPs with temperature values was depicted in Figure 11. According to Figure 11, the uptake amounts at equilibrium increased up to 35 °C, and after that, it slightly decreased by the further increase in temperature. So, the optimum temperature was determined as 35 °C for Cu^{2+} ion adsorption onto IO-NPs.

3.4 Equilibrium, kinetic, and mass transfer modeling

3.4.1 Equilibrium modeling

The adsorption isotherm models could be used for modeling the relationships between adsorbate and adsorbent at adsorption equilibrium. The well-established isotherm models of Langmuir and Freundlich were applied to the experimental equilibrium data at different temperatures.

The Langmuir model, that is applicable for monolayer adsorption onto the exactly homogeneous surface with limited availability of identical sites and with too weak interaction between adsorbed molecules is presented by Equation (3):

$$q_e = \frac{Q^o.b.C_e}{1+b.C_e} \quad (3)$$

Freundlich isotherm defines the heterogeneous surface energies by multilayer adsorption, and it is stated by Equation (4) [16]:

$$q_e = K_F.C_e^{(1/n)} \quad (4)$$

The isotherm constants calculated from the linearized isotherm equations along with the regression coefficients were presented in Table 2. Also, the isotherm graph at optimum temperature was plotted in Figure 12.

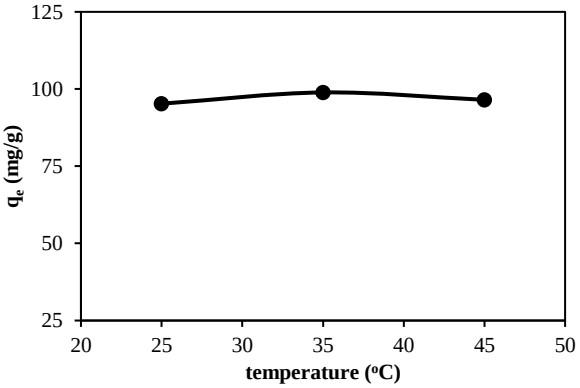

Figure 11. Effect of temperature (initial pH=5, C_o=100 mg/L, X_o=1 g/L)

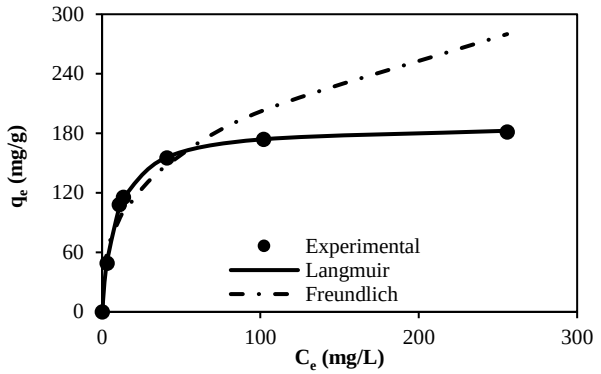

Figure 12. The isotherm graphs (q_e vs C_e) (initial pH=5, T=35°C, X_o=1 g/L)

As shown in Table 2, higher regression coefficients (R^2 >0.99) and lower ARE of the Langmuir isotherm model indicated that Cu^{2+} adsorption equilibrium data were well-described by the Langmuir isotherm model. The consistency between experimental q_e values and calculated q_e values from Langmuir isotherm model also approved that the experimental equilibrium data of Cu^{2+} adsorption best fitted to the Langmuir isotherm model. It can be concluded that Cu^{2+} adsorption onto IO-NPs was monolayer in nature. It meant that only one Cu^{2+} ion could adsorb onto the active sites of the adsorbent surface. Therefore, no further adsorption could take place at that site on the surface of the adsorbent. Besides, as it was expected from the results of temperature effect (Figure 11) that Q^o values were close to each other and the maximum Q^o value (188.68 mg/g) was obtained at optimum temperature.

The comparison of Q^o values of various types of iron nanoparticles for Cu^{2+} adsorption was shown in Table 1. Accordingly, it was seen that IO-NPs had relatively higher adsorption capacity compared with the iron-containing adsorbents reported in the literature.

Table 1. The maximum monolayer adsorption capacity values (Q^o) of various types of iron nanoparticles in the literature

Adsorbent	**Q^o (mg/g)**	**Reference**
$NiFe_2O_4$ magnetic nanoparticles	200.00	[18]
Fe_3O_4-NPs	188.68	This study
Magnetic nanoparticles coated by chitosan	96.15	[19]
Fe–Fe_3O_4/GO	90.90	[20]
Nano-scaled zerovalent iron	40.82	[21]
Amino functionalized Fe_3O_4@SiO_2 nanoparticles	29.85	[22]
Amino-functionalized magnetic nanosorbent	25.77	[23]

3.4.2 Mass transfer modeling

Several steps, such as intraparticle diffusion, external diffusion, and adsorption, or a combination of more than one step can occur during the transport of adsorbate molecules from the liquid phase to the adsorbent surface. The external resistance greatly reduces the process at highly-stirred systems that the stirring rate effect is unremarkable. Also, the effect of intraparticle resistances can be reduced by decreasing the size of adsorbent, in other words by using nano-sized materials. Weber-Morris intraparticle diffusion model is stated by Equation (5);

$$q_t = K_i.t^{0.5} + I \quad (5)$$

The intraparticle diffusion rate constant (K_i), and I value corresponded to external diffusion are calculated from the slope and intercept value of the plot of q_t vs. $t^{0.5}$ give, respectively. According to the theory of the model, if the plot of q_t vs. $t^{0.5}$ is a straight line and it passes through the origin, the adsorption system is controlled by only intraparticle diffusion. Conversely, if the plot is also linear but it has an intercept value, both intraparticle and film diffusion take place in the adsorption system [17]. Table 3 presented the Weber-Morris model parameters with regression coefficients of Cu^{2+} ion adsorption onto IO-NPs. According to Table 3, the model plots were linear (R^2>0.99) and also had intercept values (I); thus, the adsorption of Cu^{2+} ion onto IO-NPs followed both intraparticle and film diffusion.

3.4.3 Kinetic Modeling

It is required to assess the adsorption process kinetics for selecting the optimum running conditions for batch processes. The kinetic parameters are useful for the estimation of the adsorption rate and give information for modeling the processes.

The widely used kinetic models for the adsorption processes are the pseudo first order and the pseudo second order kinetic models. The adsorption kinetics was elucidated by correlating the adsorption kinetic data of the Cu^{2+} onto IO-NPs using the linear forms of the pseudo first order and the pseudo second order kinetic models that were given in following Equations 6 and 7, respectively [24].

$$\left[\log(q_e - q_t) = \log(q_e) - \frac{k_1 t}{2.303}\right] \quad (6)$$

$$\left[\frac{t}{q_t} = \frac{1}{qe^2 k_2} + \frac{t}{qe}\right] \quad (7)$$

Table 2. The constants of the adsorption isotherm models (initial pH=5.0, X_o=1.0 g/L)

T (°C)	Langmuir isotherm model $(1/q_e)=[(1/(Q^o.b).(1/C_e)] + (1/Q^o)$				Freundlich isotherm model $\ln(q_e)=\ln(K_F)+(1/n).\ln(C_e)$			
	Q^o (mg/g)	b (L/mg)	R^2	ARE	K_F (mg/g)/(L/mg)1/n)	n	R^2	ARE
25	181.8182	0.1316	0.991	5.9947	40.2067	0.3351	0.947	10.2815
35	188.6792	0.1165	0.999	0.7109	40.5460	0.3485	0.891	20.7332
45	185.1852	0.07397	0.994	2.2514	47.7673	0.2757	0.927	14.5122

[$ARE=(100/n).\Sigma_1^n (q_{e,cal}-q_{e,exp})/(q_{e,exp})$]

For Cu^{2+}adsorption onto IO-NPs, the kinetics model parameters and R^2 values were exhibited in Table 4 (a) and (b). From Table 4 (a) and (b), the adsorption kinetics of Cu^{2+} onto IO-NPs was well-defined by the pseudo second order kinetic model due to the consistency of the experimental and calculated q_e values and high regression coefficients than the pseudo first order model at all initial Cu^{2+} ion concentrations.

Table 3. The parameters of Weber-Morris model (initial pH=5.0, T=35°C, X_o=1.0 g/L)

C_o (mg/L)	K_i (mg/g.min$^{0.5}$)	Intercept (I)	R^2
52.0566	0.0103	47.39	0.990
119.0377	4.2274	74.50	0.994
145.4717	4.7436	80.18	0.993
275.6981	5.8955	93.69	0.995

Table 4.a. The parameters of the pseudo first order kinetic model (initial pH=5.0, T=35°C, X_o=1.0 g/L)

C_o (mg/L)	$q_{e,exp}$ (mg/g)	Pseudo first order		
		k_1*10^3 (min^{-1})	$q_{e,cal1}$ (mg/g)	R^2
52.0566	56.98	24.41	41.96	0.952
119.0377	118.94	24.41	68.36	0.882
145.4717	143.49	20.73	100.74	0.965
196.0755	160.60	16.58	120.67	0.821
275.6981	173.81	16.58	128.53	0.943
437.2075	181.43	1.45	128.17	0.871

Table 4.b. The parameters of the pseudo second order kinetic model (initial pH=5.0, T=35°C, X_o=1.0 g/L)

C_o (mg/L)	$q_{e,exp}$ (mg/g)	Pseudo second order		
		k_2*10^4 (g/mg.min)	$q_{e,cal2}$ (mg/g)	R^2
52.0566	56.98	15.39	53.69	0.991
119.0377	118.94	12.50	114.66	0.997
145.4717	143.49	7.74	138.66	0.993
196.0755	160.60	4.85	149.91	0.991
275.6981	173.81	3.04	157.26	0.991
437.2075	181.43	6.29	173.01	0.990

4. Conclusions

The present work revealed that iron oxide nanoparticles (IO-NPs) could be synthesized through the fast and facile biosynthesis method using *Enteromorpha spp.* extract as a biological reductant/capping agent. Algae are abundant resources exist in both fresh and saltwater; also, they cause water pollution. This study showed that they can be converted into economic value by evaluating them in nanoparticle biosynthesis and also the water pollution arising from algae can be reduced by this means.

Acknowledgment

This work supported by the Scientific Research Projects Management of Mersin University is gratefully acknowledged (Project number: 2018-1-TP2-2779), Turkey.

Nomenclature

- b : Freundlich isotherm model constant (L/mg)
- C_e : Residual Cu^{2+} ion concentration at equilibrium (mg/L)
- C_o : Initial Cu^{2+} ion concentration (mg/L)
- K_F : Freundlich constant indicating adsorption capacity ((mg/g)/(L/mg)$^{1/n}$)
- K_i : Rate constant of intraparticle diffusion (mg/g.min$^{1/2}$)
- k_1 : Rate constant of pseudo first order kinetic model (1/min)
- k_2 : Rate constant of pseudo second order kinetic model (g/mg.min)
- I : Intercept value of Weber-Morris plot
- q_e : Uptake amount per unit mass of adsorbent at equilibrium (mg/g)
- q_{e,cal_1} : Calculated uptake amount per unit mass of adsorbent from pseudo first order kinetic model (mg/g)
- q_{e,cal_2} : Calculated uptake amount per unit mass of adsorbent from pseudo second order kinetic model (mg/g)
- $q_{e,exp}$: Experimental uptake amount per unit mass of adsorbent (mg/g)
- q_t : Uptake amount per unit mass of adsorbent at any time (mg/g)
- Q^o : Maximum monolayer adsorption capacity (mg/g)

R^2 : Regression coefficient
T : Temperature (°C, K)
t : Time (min)
1/n : Freundlich constant indicating adsorption intensity

References

1. Uzunoğlu, D., and A. Özer, *Adsorption of hazardous heavy metal copper (II) from aqueous effluents onto waste material fish (Dicentrarchus labrax) scales: optimization, equilibrium, kinetics, thermodynamic, and characterization studies.* Desalination and Water Treatment, 2016. **57**(48-49): p. 22794-22798.
2. Ajouyed, O., C. Hurel, M. Ammari, L.B. Allal, and N. Marmier, *Sorption of Cr (VI) onto natural iron and aluminum (oxy) hydroxides: effects of pH, ionic strength and initial concentration*. Journal of Hazardous. Materials, 2010. **174**(1): pp. 616-622.
3. Abhalaxmi, S., and S.K. Sahoo, *Magnetic nanoparticles: a novel platform for cancer theranostics*, Drug Discovery Today, 2014. **19**(4): p. 474-481.
4. Mahdavi, M., F. Namvar, M.B. Ahmad, and R. Mohamad, *Green biosynthesis and characterization of magnetic iron oxide (Fe_3O_4) nanoparticles using seaweed (Sargassum muticum) aqueous extract.* Molecules, 2013. **18**(5): p.5954-5964.
5. Azizi, S., M. B. Ahmad, F. Namvar, R. Mohamad, *Green biosynthesis and characterization of zinc oxide nanoparticles using brown marine macroalga Sargassum muticum aqueous extract.* Materials Letters, 2014. **116**: p. 275-277.
6. Slinkard, K., & Singleton, V. L. *Total phenol analysis: automation and comparison with manual methods*, American journal of enology and viticulture, 1977. **28** (1), 49-55.
7. El-Kassas, H. Y., M. A. Aly-Eldeen, and S. M. Gharib, *Green synthesis of iron oxide (Fe_3O_4) nanoparticles using two selected brown seaweeds: characterization and application for lead bioremediation*. Acta Oceanologica Sinica, 2016. **35**(8): p. 89-98.
8. Shahwan, T., Sirriah, S. A., Nairat, M., Boyacı, E., Eroğlu, A. E., Scott, T. B., & Hallam, K. R. *Green synthesis of iron nanoparticles and their application as a Fenton-like catalyst for the degradation of aqueous cationic and anionic dyes.* Chemical Engineering Journal, 2011.**172**(1):p. 258-266.
9. Iram, M., C. Guo, Y. Guan, A. Ishfaq, and H. Liu, *Adsorption and magnetic removal of neutral red dye from aqueous solution using Fe_3O_4 hollow nanospheres.* Journal of Hazardous Materials, 2010. **181**(1): p. 1039-1050.
10. Döker, O., Ergüt M. *Recovery of Bioactive Phenolic Compounds from Lemon (Citrus limon (L.) Burm. f.) and Orange (Citrus Sinensis L. Osbeck) Pomaces.* Chemical and Process Engineering Research, 2017. 51:p.18-33.
11. Kumar, K. M., Mandal, B. K., Kumar, K. S., Reddy, P. S., & Sreedhar, B. *Biobased green method to synthesise palladium and iron nanoparticles using Terminalia chebula aqueous extract*. Spectrochimica Acta Part A: Molecular and Biomolecular Spectroscopy, 2013. 102: p. 128-133.
12. Ganesan, K., K. Suresh Kumar, and PV Subba Rao. *Comparative assessment of antioxidant activity in three edible species of green seaweed, Enteromorpha from Okha, Northwest coast of India*. Innovative food science & emerging technologies, 2011. **12**(1): p.73-78.
13. Akköz, C., Arslan, D., Ünver, A., Özcan, M. M., and Yilmaz, B. *Chemical composition, total phenolic and mineral contents of Enteromorpha intestinalis (L.) Kütz. and Cladophora glomerata (L.) Kütz. seaweeds.* Journal of Food Biochemistry, 2011. **35** (2): p.513-523.
14. Uzunoğlu, D., N. Gürel, N. Özkaya, A. Özer. *The single batch biosorption of copper (II) ions on Sargassum acinarum.* Desalination and Water Treatment, 2014. **52**(7-9): p. 1514-1523.
15. Brungesh, K. V., B. M. Nagabhushana, M.N.K. Harish, and R. Hari Krishna, *An Efficient Removal of Toxic Cr (VI) from Aqueous Solution by MnO2 Coated Polyaniline Nanofibers: Kinetic and Thermodynamic Study*. Journal of Environmental Analysis Toxicology, 2017. **7**(442): p. 2161-0525.
16. Fan, L., C. Luo, M. Sun, X. Li, F. Lu, and H. Qiu, *Preparation of novel magnetic chitosan/graphene oxide composite as effective adsorbents toward methylene blue*. Bioresource Technology, 2012. **114**: p. 703-706
17. Benhouria, A., M. A. Islam, H. Zaghouane-Boudiaf, M. Boutahala, B.H. Hameed, *Calcium alginate–bentonite–activated carbon composite beads as highly effective adsorbent for methylene blue.* Chemical Engineering Journal, 2015. **270**: p.621-630.
18. Moeinpour, F., and S. Kamyab. *Adsorption characteristics of Cu^{2+} on $NiFe_2O_4$ magnetic nanoparticles*. Journal of Water Reuse and Desalination, 2015. **5**(2): p. 223-230.
19. Zhou, Y. T., H. L. Nie, C. Branford-White, Z. Y. He, and L. M. Zhu. *Removal of Cu^{2+} from aqueous solution by chitosan-coated magnetic nanoparticles modified with α-ketoglutaric acid.* Journal of Colloid and Interface Science, 2009. **330**(1): p. 29-37.
20. Le, G. H., A. Q. Ha, Q. K. Nguyen, K. T. Nguyen, P. T. Dang, H. T. Tran, and T. A. Vu. *Removal of Cd^{2+} and Cu^{2+} ions from aqueous solution by using Fe–Fe3O4/graphene oxide as a novel and efficient adsorbent.* Materials Research Express, 2016. **3**(10): p. 105603.

21. Dada, A. O., F. A. Adekola, and E. O. Odebunmi. *Kinetics, Isotherms and Thermodynamics Studies of Sorption of Cu^{2+} onto Novel Zerovalent Iron Nanoparticles.* Covenant Journal of Physical and Life Sciences, 2014. **2**(1): p. 24-53.

22. Shoueir, K. R., A. Sarhan, A. M. Atta, and M. A. Akl. *Adsorption studies of Cu^{2+} onto poly (vinyl alcohol)/poly (acrylamide-co-N-isopropylacrylamide) core–shell nanogels synthesized through surfactant-free emulsion polymerization.* Separation Science and Technology, 2016. **51**(10): p. 1605-1617.

23. Hao, Y. M., C. Man, and Z. B. Hu. *Effective removal of Cu (II) ions from aqueous solution by amino-functionalized magnetic nanoparticles.* Journal of Hazardous Materials, 2010. **184** (1): p. 392-399.

24. Yan, Y., Q. An, Z. Xiao, W. Zheng, and S. Zhai, *Flexible core-shell/beadlike alginate@PEI with exceptional adsorption capacity, recycling performance toward batch and column sorption of Cr (VI),* Chemical Engineering Journal, 2017. **313**: p. 475-486.